Applied Catalysis B: Environmental 325 (2023) 122305

Contents lists available at ScienceDirect

Applied Catalysis B: Environmental

journal homepage: www.elsevier.com/locate/apcatb

Ruthenium-doped 3D Cu_2O nanochains as efficient electrocatalyst towards hydrogen evolution and hydrazine oxidation

Pei Shen [a,c], Bowen Zhou [a,e], Zhi Chen [a], Weiping Xiao [b], Yunlei Fu [a], Jun Wan [c], Zexing Wu [a,d,*], Lei Wang [a,c,d,*]

[a] Key Laboratory of Eco-chemical Engineering, International Science and Technology Cooperation Base of Eco-chemical Engineering and Green Manufacturing, Qingdao University of Science and Technology, Qingdao 266042, PR China
[b] College of Science, Nanjing Forestry University, Nanjing 210037, PR China
[c] College of Environment and Safety Engineering, Qingdao University of Science and Technology, Qingdao 266042, PR China
[d] College of Chemistry and Molecular Engineering, Qingdao University of Science and Technology, Qingdao 266042, PR China
[e] Beijing Key Laboratory of Materials Utilization of Nonmetallic Minerals and Solid Wastes, National Laboratory of Mineral Materials, School of Materials Science and Technology, China University of Geosciences, Beijing 100083, PR China

ARTICLE INFO

Keywords:
Electrocatalyst
Hydrogen evolution reaction
Hydrazine oxidation reaction
Water-splitting
Cu_2O

ABSTRACT

The sluggish kinetics of oxygen evolution reaction (OER) hampers the conversion of renewable energies into hydrogen through an electrocatalytic process. Then, the hydrazine oxidation reaction (HzOR) is a promising anodic reaction to substitute OER, which can decrease the water-splitting voltage. Herein, self-supported ruthenium-doped cuprous oxide nanochains were synthesized on commercial copper foam (Ru-Cu_2O/CF). The Ru-Cu_2O/CF provides superior hydrogen evolution reaction (HER) and HzOR performances owing to its specific morphology, superhydrophilic surface, porous support and Ru doping. When used in alkaline or neutral electrolytes, the Ru-Cu_2O/CF is capable of driving 10 mA cm^{-2} only at 31 and 51 mV, respectively. In HzOR, it is possible to achieve a superlow potential of − 41 mV at 10 mA cm^{-2}. In an electrolytic cell with a Ru-Cu_2O/CF both as cathode and anode, a voltage of 17.4 mV is needed to reach 10 mA cm^{-2}, which is powered by renewable energies.

1. Introduction

Fossil fuel consumption has prompted research into clean and sustainable energy sources [1–4]. As an environmentally friendly and high-energy-density secondary energy source, hydrogen has attracted more attention [5–7]. At present, steam alcohol reforming and coal gasification have been mainly used to produce hydrogen, but they cannot avoid using fossil fuels and producing carbon dioxide [8,9]. Electrocatalytic water splitting is one of the most prospective ways to produce hydrogen because of its advantages of non-polluting and zero-emission, especially in combination with renewable energy [10–12]. Normally, the overall water splitting (OWS) process consists of two half-reactions, HER ($4\ H^+ + 4e^- \rightarrow 2\ H_2$) on the cathode and OER ($4OH^- \rightarrow O_2 + 2\ H_2O + 4e^-$) on the anode [13–15]. However, the OER process is the limiting step of OWS due to its slow kinetics, specifically in the associated proton-coupled electron transfer step, which severely limits the practical application [16–19]. Even though many outstanding electrocatalysts have been developed, OER still requires higher voltage to drive [20–22]. Recently, some thermodynamic favorable molecular processes or economically attractive reactant oxidation reactions have been commonly used as an energy efficiency reduction strategy to replace the sluggish OER reactions. Such as methanol [23,24], urea [25,26], ethanol [27], nitrogen [28] and hydrazine [29–31] oxidation reaction. Among them, the theoretical potential of HzOR is only − 330 mV which is much smaller than OER [32–36]. Hydrogen production efficiency can be improved with this substitution strategy, on the other hand, the overall hydrazine splitting (OHzS) products are H_2 and N_2, which are safer than OWS in the membrane-free cell [37–40]. Therefore, the HER and HzOR bifunctional electrocatalysts have become a research hotspot. Nevertheless, the preparation of efficient and durable electrocatalysts for relevant reactions is still a challenging task.

Over the past several decades, many noble metal-based catalysts

* Corresponding authors at: Key Laboratory of Eco-chemical Engineering, International Science and Technology Cooperation Base of Eco-chemical Engineering and Green Manufacturing, Qingdao University of Science and Technology, Qingdao 266042, PR China.
E-mail addresses: splswzx@qust.edu.cn (Z. Wu), inorchemwl@126.com (L. Wang).

https://doi.org/10.1016/j.apcatb.2022.122305
Received 17 October 2022; Received in revised form 3 December 2022; Accepted 17 December 2022
Available online 24 December 2022

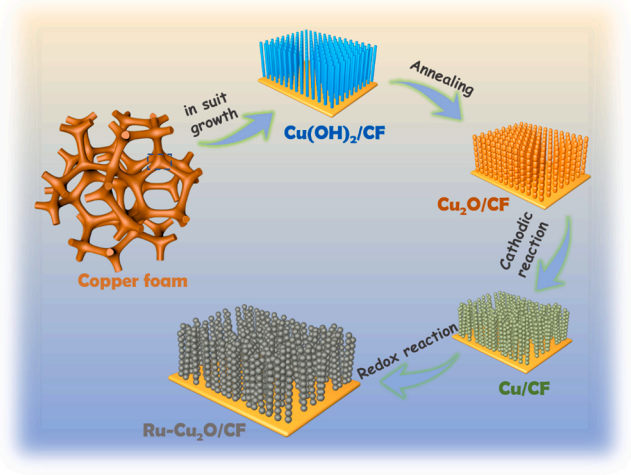

Fig. 1. Schematic illustration of the preparation process of Ru-Cu_2O/CF.

with attractive electrocatalytic performance, for instance, Pt, IrO_2 and RuO_2, have already been discovered [41–43]. These catalysts always have excellent properties, but the high price and lack of stability under harsh conditions have severely hindered their widespread industrial use [44–46]. Therefore, simultaneous reduction of precious metal content and improvement of catalytic performance and stability are necessary for large-scale hydrogen production. It is an attractive method to achieve complementary advantages between multiple components by coupling with non-precious transition metals. And copper (Cu) is a transition metal which is abundant on the earth [47–50]. Due to its multiple redox states (Cu^0, Cu^{+1}, Cu^{+2} and Cu^{+3}), Cu-based nanomaterials are considered not only a potential HER catalyst but also an OWS catalyst [51–53]. Among them, copper foam (CF) is an excellent electrocatalytic material with a three-dimensional (3D) structure that facilitates air bubble discharge and contact between the electrolyte and the material surface [54–57]. At present, many noble metal catalysts built on CF have shown excellent performance. For instance, Tran et al. synthesized hierarchical 3D Cu nanowires catalysts, with Pt nanodots deposited on them. The increased active area, and strong interaction between Cu and Pt phases, produce an high-efficiency OWS process [58]. Xu et al. reported Rh Single-atom site catalysts on CuO nanowire arrays (CuO NAs) as electrodes for alkaline water splitting. In this work,

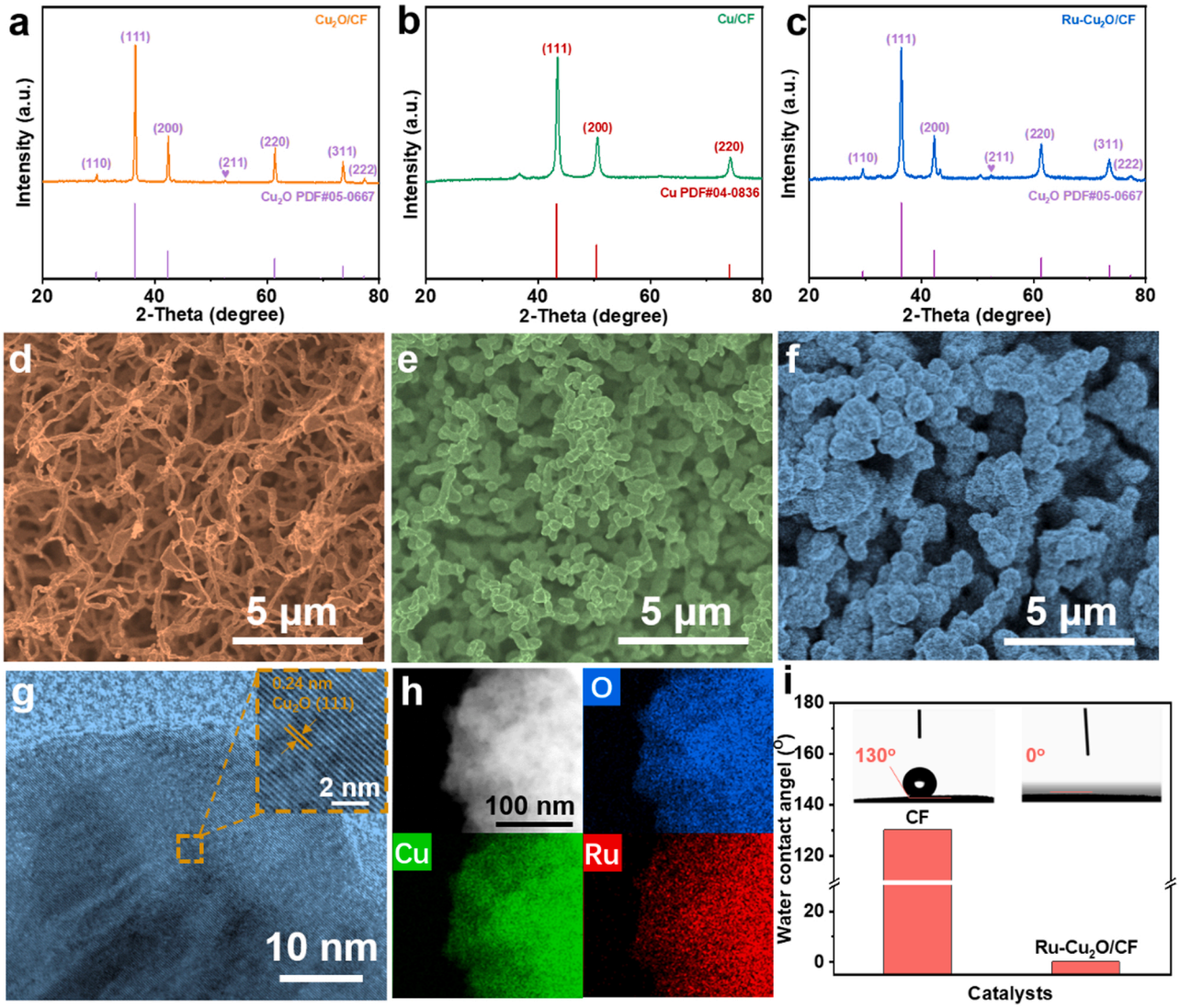

Fig. 2. (a-c) XRD patterns and (d-f) SEM images of the Cu_2O/CF, Cu/CF and Ru-Cu_2O/CF. (g) HRTEM image and (h) EDS-mapping of the Ru-Cu_2O/CF. (i) Water contact angles of CF and Ru-Cu_2O/CF.

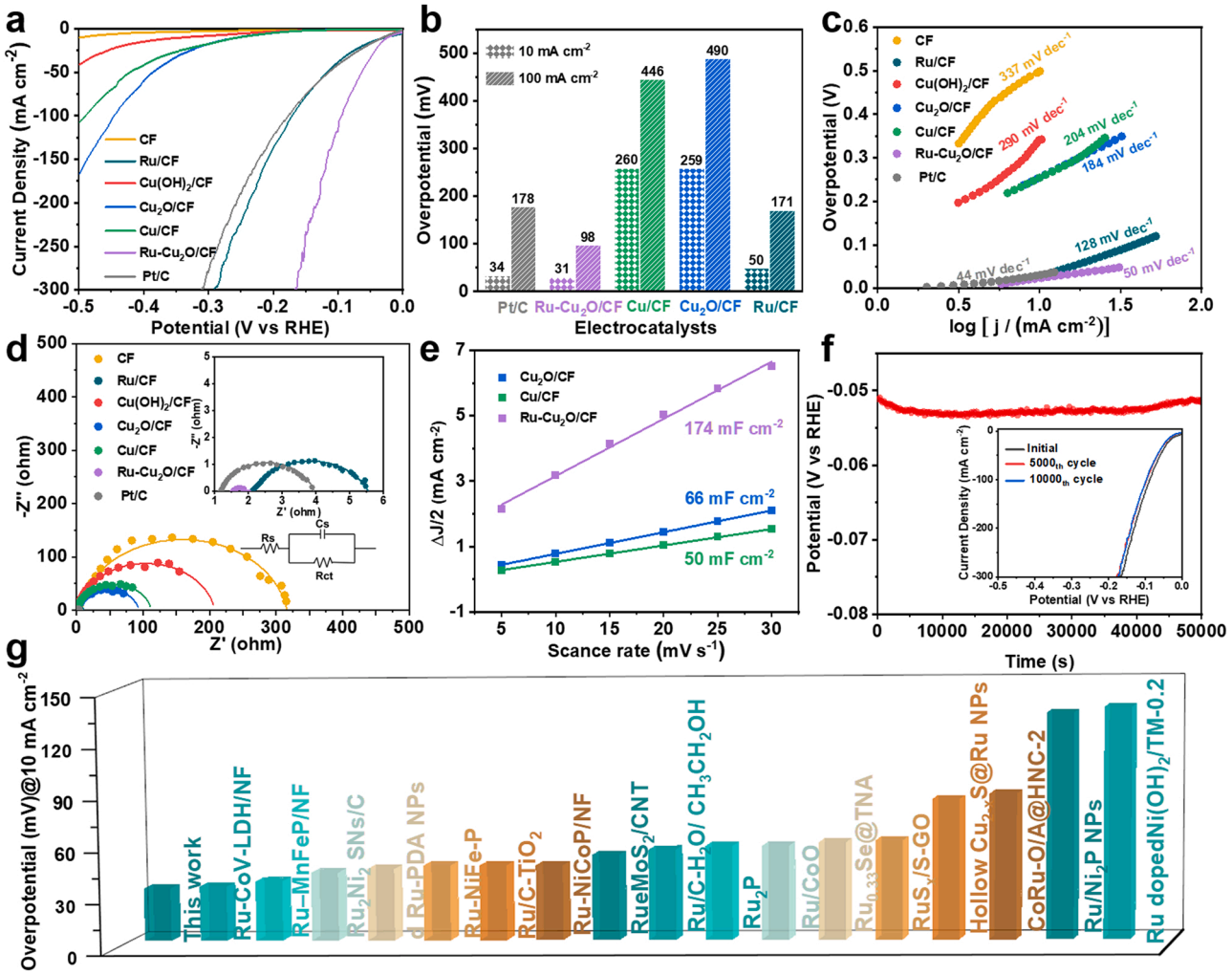

Fig. 3. HER performances of the Ru-Cu_2O/CF and the counterparts in alkaline solution. (a) The LSV curves. (b) Overpotential at the 10 mA cm^{-2} and 100 mA cm^{-2} current density. (c) Tafel slopes. (d) Nyquist plots. (e) Electrochemical double-layer capacitances (C_{dl}). (f) The chronopotentiometry curves for the Ru-Cu_2O/CF measured at 10 mA cm^{-2} without iR-compensation. (Insert: HER polarization curves after different CV cycles.) (g) Comparison with previously reported overpotentials of Ru-based catalysts at 10 mA cm^{-2}.

the performance of M SACs-CuO NAs/CF (M = Ru, Ir, Os, Au) has also been evaluated. compared with CuO NAs/CF, these M SACs-CuO NAs/CF catalysts all show enhanced OER performance, providing evidence that noble metal SACs doped on CuO NAs can availably increase electrocatalytic toward water splitting [59]. Ruthenium (Ru) is a relatively inexpensive precious metal. With an excellent ability to adsorb-desorb H* , it is located at the top and center of the HER volcano diagram [60,61]. Ru doping can enhance the adsorption of Cu for H* and thus enhance HER performance [62]. Besides, numerous Ru-based catalysts have shown highly activity for HzOR in previous studies [63,64]. For example, Wang et al. reported Ru/MPNC composite catalysts exhibits superior bifunctional HER and HzOR activity, outperforming commercial Pt/C composites [65]. Therefore, fabricated Cu-based catalysts coupling with Ru on the CF, can exploit not only exploit structural advantages but also the interaction between Cu and Ru phases, thus multifunctional active sites can be probably produced.

In this work, a nanochain morphology catalysts, stacked by ruthenium-doped cuprous oxide nanosphere, was prepared onto copper foam, which is prepared via surface oxidation, annealing, cathode reduction and redox reaction. The prepared Ru-Cu_2O/CF exhibits outstanding bifunctional catalytic activity for HER and HzOR. Due to the unique morphology, surface superhydrophilicity, and Cu-Ru interaction, electrocatalytic activity is highly enhanced. Two-electrode electrolytic cell only requires a voltage of 17.4 mV to driving 10 mA cm^{-2} current density with Ru-Cu_2O/CF as both anode and cathode in 1.0 M KOH and 0.5 M N_2H_4 solution. The prepared Ru-Cu_2O/CF shows great potential for energy-saving hydrogen production compared to the OWS system.

2. Experimental section

2.1. Synthesis of $Cu(OH)_2$/CF

In a typical synthesis, six pieces of CF (1 ×1.5 cm^2) were placed in an aqueous solution (40 mL) retaining 20 min, which containing NaOH (3.2 g) and $(NH_4)_2S_2O_8$ (1.0 g). The product was named $Cu(OH)_2$/CF. After being washed with DI water three times, these pieces of $Cu(OH)_2$/CF were dried at 60 °C.

2.2. Synthesis of Cu/CF

An annealing procedure was conducted at 600 °C for 4 h with Ar atmosphere on the $Cu(OH)_2$/CF, which was transformed into Cu_2O/CF. The prepared Cu_2O/CF was electrochemically reduced to Cu/CF at −0.6 V vs. RHE for 0.5 h.

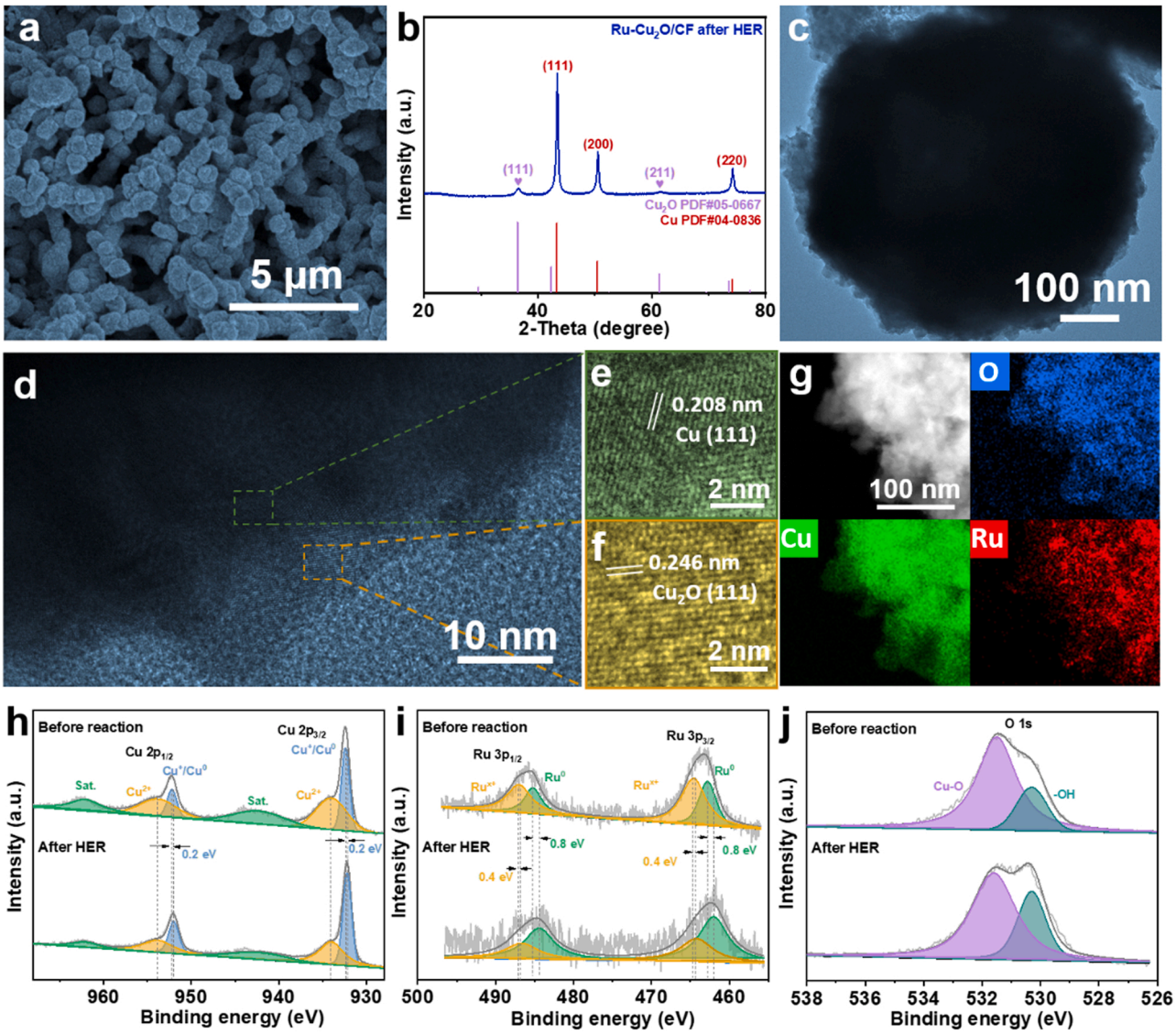

Fig. 4. (a) SEM image, (b) The XRD pattern, (c) TEM and (h) HRTEM images of Ru-Cu_2O/CF after the durability test. (e-f) Partial enlarged view of the HRTEM image. (g) EDS-mapping of the Ru-Cu_2O/CF after the durability test. (h-j) The XPS spectrum of Cu, Ru and O of Ru-Cu_2O/CF before and after the durability test.

2.3. Synthesis of Ru-Cu_2O/CF

The Ru-Cu_2O/CF was prepared by immersing one piece of Cu/CF into 10 mg mL^{-1} $RuCl_3 \bullet xH_2O$ aqueous solution, and stirring for 5 h at 25 °C. After being washed with DI water three times, these of Ru-Cu_2O/CF were dried at 60 °C. By the same method, used CF to directly produce Ru/CF.

2.4. Electrochemical measurements

The HER electrochemical tests were performed in a CHI 760E electrochemical workstation with a typical three-electrode system. The reversible hydrogen electrode (RHE) and carbon rod served as the reference and counter electrode, respectively. Gamry Reference 3000 electrochemical workstation was used for the HzOR electrochemical measurements with a silver chloride electrode as the reference electrode. With an iR compensation of 95%, the linear sweep voltage (LSV) curves were taken using a sweep rate of 5 mV s^{-1}. A frequency range of 0.1 Hz ~100 kHz and an AC amplitude of 5 mV are used tested electrochemical impedance spectroscopy of the samples in 1.0 M KOH at − 0.121 V (vs. RHE). The value of the double layer capacitance (C_{dl}) was calculated from the CV curves, which were measured in a scan rate of 5, 10, 15, 20, 25 and 30 mV s^{-1}, respectively.

3. Results and discussion

3.1. Characterization of Ru-Cu_2O/CF

The fabrication of the Ru-Cu_2O/CF is clearly shown in Fig. 1. Firstly, a layer of uniform $Cu(OH)_2$ nanowires is grown on the smooth copper hydroxide surface by corrosion and surface oxidation. Then, the Cu $(OH)_2$ nanowires are annealed into Cu_2O nanowires at high temperatures in Ar atmosphere. In the third step, the Cu_2O is reduced to Cu by electrochemical reduction. Finally, the Cu nanochains are converted into Ru-doped Cu_2O nanochains in ruthenium trichloride solution by stirring at room temperature. In this case, since Cu has a lower standard reduction potential than Ru, the galvanic replacement reaction of Cu and Ru^{3+} will take place and then be generated as Cu_2O in the presence of O_2.

The XRD patterns of powder, scraped from the Cu foam substrate of the as-prepared samples, are demonstrated in Fig. 2**a**, **b** and **c**. The powder of Cu_2O/CF exhibits several sharp peaks at an angel (2θ) of

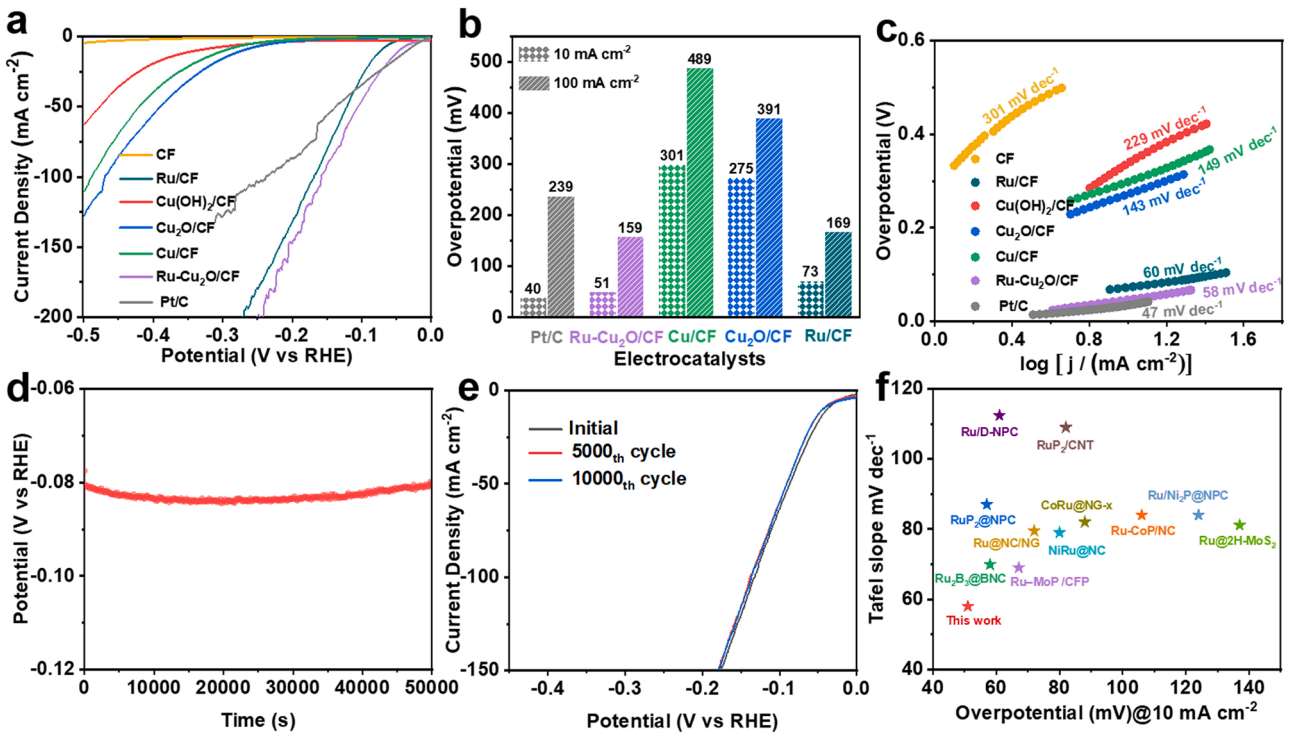

Fig. 5. HER performance of the Ru-Cu_2O/CF and the counterparts in neutral solution. (a) The LSV curves. (b) Overpotential at the current densities of 10 mA cm^{-2} and 100 mA cm^{-2}. (c) Tafel slopes. (d) The chronopotentiometry curves for Ru-Cu_2O/CF were measured at 10 mA cm^{-2} without iR-compensation. (e) HER polarization curves for Ru-Cu_2O/CF after different CV cycles. (f) Comparison of overpotentials at 10 mA cm^{-2} and Tafel slopes of the previously reported Ru-based catalysts.

29.5°, 36.4°, 42.3°, 61.3°, 73.5° and 77.3°, which are attributed to the crystal planes of (110), (111), (200), (220), (311) and (222) for Cu_2O (PDF No. 05–0667), in Fig. 2**a**. In addition, Fig. 2**b** shows the XRD pattern of Cu/CF. It shows that the XRD peaks are respectively located in 43.2°, 50,4° and 74.1°, which corresponds to the planes of (111) (200) and (220) for Cu (PDF No. 04–0836). That means, after 30 min electrochemical reduction process, the Cu_2O phase was completely changed into a Cu phase. After the redox reaction process, the Ru-Cu_2O/CF contains the phases of Cu_2O (PDF No. 05–0667), in the Fig. 2**c**. The micromorphology of various samples is characterized via SEM and TEM. Fig. S1 shows the SEM image of $Cu(OH)_2$/CF, numerous nanowires uniformly covering on the surface of the Cu foam can be observed. Fig. 2**d** and S2 illustrate that the $Cu(OH)_2$ nanowires transform into thin and curled Cu_2O nanowires after annealing process. Unlike the Cu_2O nanowires, Cu/CF presents a nanochains structure (Fig. 2**e** and S3). Obviously, Ru-Cu_2O/CF exhibits similar morphology with Cu/CF but the surface converts roughly after react with Ru (Fig. 2**f** and S4). TEM image verifies the nanochains are composed of nanoparticles (Fig. S5). The high-resolution TEM (HRTEM) in Fig. 2**g**, which displays clear fringes with a lattice plane distance of 0.240 nm assigning to the (111) plane of Cu_2O. The energy-dispersive X-ray spectroscopy (EDS) elemental mapping (Fig. 2**h**) displays the uniformly distribution of Cu, Ru and O elements in Ru-Cu_2O/CF. Furthermore, we used the X-ray photoelectron spectroscopy (XPS) to analyzing chemical composition and structure of the samples. Fig. S6a shows fine spectra of Cu for Cu_2O/CF, Cu/CF and Ru-Cu_2O/CF. Two peaks of Cu $2p_{3/2}$ and Cu $2p_{1/2}$ for Cu^+ or Cu^0 are located at 932.62 eV and 952.37 eV [66–68]. The XRD and HRTEM analysis show that the oxidation state of Cu changes evidently but no significant variation in the XPS spectrum is observed because the binding energies overlap between Cu^+ and Cu^0 [69]. The signals at 935 eV and 954.75 eV can be assigned to Cu^{2+}, owing to the oxidation by air [70,71]. The XPS spectra of Ru are shown in Fig. S6b. No signals of Ru $3p_{3/2}$ and Ru $3p_{1/2}$ are observed in Cu_2O/CF and Cu/CF. Two peaks at 462.8 eV and 485.2 eV are detected in Ru-Cu_2O/CF which responded to Ru^0 [72,73]. Meanwhile, the signals at 464.6 eV and 487 eV can be assigned to Ru^{x+}[74,75]. As for the O 1 s XPS spectra (Fig. S6c), two peaks at 530.3 eV and 531.6 eV can be labeled as Cu-O bonds and -OH bonds [67,69]. The water contact angle decreased from 130° (CF) to 0° (Ru-Cu_2O/CF), demonstrating the super hydrophilic surface of Ru-Cu_2O/CF which benefits the mass transport and boosts the reaction kinetics during the electrocatalytic process (Fig. 2**i**).

3.2. *Hydrogen evolution reaction performance*

All electrochemical measurements of the samples were performed on a standard three-electrode calibration system with 1.0 M KOH as electrolyte. As exhibited in the Fig. 3**a**, the bare CF substrate and the Cu $(OH)_2$/CF presents almost negligible HER activity. Meanwhile, as a contrast of Ru/CF, Cu_2O/CF and Cu/CF, the Ru-Cu_2O/CF exhibits sharp improvement in HER performance, even surpassing the commercial Pt/C. Based on Fig. 3b, Ru-Cu_2O/CF has a lower overpotential of 31 mV at 10 mA cm^{-2} than commercial Pt/C (34 mV) and the reference catalysts (Ru/CF 50 mV, Cu/CF 260 mV and Cu_2O/CF 259 mV). Moreover, it displays the smallest overpotential of 98 mV to reach 100 mA cm^{-2} among the studied catalysts. Tafel slope is a valuable parameter for assessing electrocatalyst kinetics and reaction pathway. As displayed in Fig. 3**c**, the Ru-Cu_2O/CF displayed a Tafel slope of 50 mV dec^{-1}, which is much lower than Cu/CF (204 mV dec^{-1}), Ru/CF (128 mV dec^{-1}), Cu_2O/CF (184 mV dec^{-1}) and $Cu(OH)_2$/CF (290 mV dec^{-1}), indicating its favorable HER kinetic. It is well known that electrical conductivity and electron transfer rate are important factors on affecting the catalytic activity. The Nyquist plots of samples reveal that the Ru-Cu_2O/CF owns minimum charge transfer resistance (R_{ct}) (Fig. 3**d**), consistent with HER performance. In order to compare the electrochemical active surface area (ECSA) of the prepared samples, cyclic voltammetry (CV) was used to calculate the double layer capacitance (C_{dl}) values. (Fig. S7). The C_{dl} value of Ru-Cu_2O/CF (174 mF cm^{-2}) has been improved a lot than that of Cu_2O/CF (66 mF cm^{-2}) and Cu/CF (50 mF cm^{-2}) (Fig. 3**e** and S7),

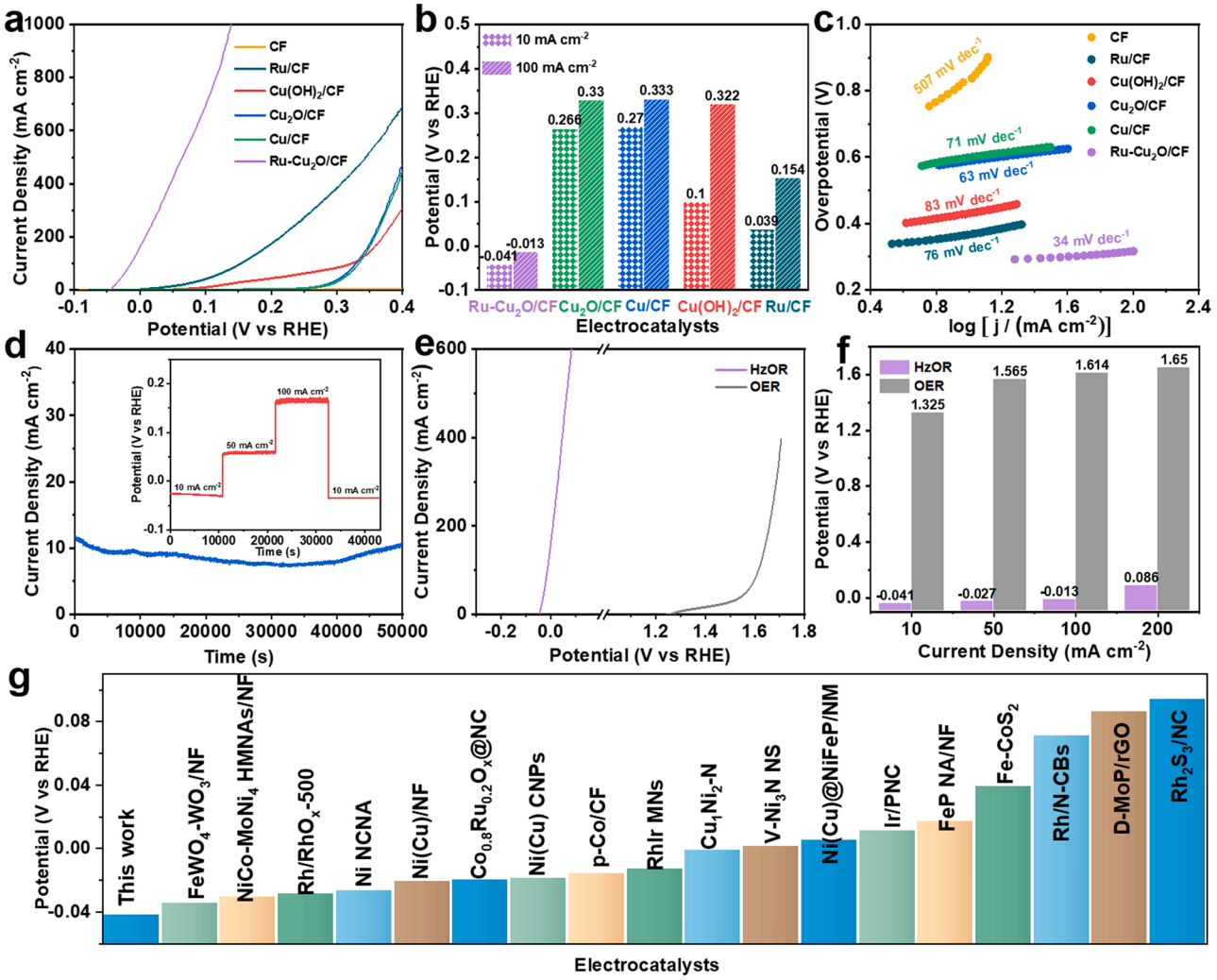

Fig. 6. HzOR performance of the Ru-Cu_2O/CF and the counterparts in alkaline solution. (a) The LSV curves. (b) Overpotential at 10 mA cm^{-2} and 100 mA cm^{-2}. (c) Tafel slopes. (d) The chronoamperometry curve for Ru-Cu_2O/CF at the voltage of − 0.006 V (vs. RHE). (The inset: The multi-steps chronopotentiometry curves for Ru-Cu_2O/CF tested at different current densities without iR-compensation.) (e) The LSV curves of HzOR and OER. (f) Overpotential of HzOR and OER at 10–200 mA cm^{-2}. (g) Comparison of overpotentials at 10 mA cm^{-2} of the recently reported catalysts.

indicating that the Ru-Cu_2O/CF possess more exposed active sites. In addition, we also characterize the durableness of the Ru-Cu_2O/CF by a battery of the long-term stability test. The chronopotentiometry measure (without iR compensation) remains nearly unchanged for 50,000 s at 10 mA cm^{-2}(Fig. 3**f**). The LSV curves of Ru-Cu_2O/CF display a negligible decrease from the initial one after 5,000 and 10,000 cycles (Fig. 3**f**, inset). It is indicated that Ru-Cu_2O/CF exhibits excellent stability and has potential for industrial. In addition, further demonstrating the HER catalytic performance of Ru-Cu_2O/CF, surpassing most recently reported Ru-based catalysts in 1.0 M KOH (Fig. 3**g** and Table S1).

To investigate its stability, we conducted a series of characterizations of the sample after chronopotentiometry measurement. The SEM image reveals that the nanochains structure was maintained well after the stability test (Fig. 4**a**). Nevertheless, the XRD pattern shows that Cu_2O transformed into Cu (Fig. 4**b**). TEM image demonstrates that the morphology of the Ru-Cu_2O/CF maintained well after the durability measurement (Fig. 4**c**). A partially enlarged view of the HRTEM image shows the lattice plane distances of 0.208 nm in (Fig. 4**d** and **e**), corresponding to (111) planes of Cu. In addition, Fig. 4**f** shows the (111) plane of Cu_2O with lattice plane distances of 0.246 nm. The EDX-mapping shows the nanosphere contains the expected elements Cu, Ru and O, which are uniform distributed over the structure (Fig. 4**g**). Fig. 4**h** shows the XPS spectrum of Cu 2p. The binding energies for Cu^+ or Cu^0 (932.2 eV and 952 eV) slightly shifted in comparison with the sample before the stability test [32,76–80], owing to the reduction of Cu_2O to Cu. For Ru 3p (Fig. 4**i**), the contents of Ru^0 species increased and Ru^{x+} decreased, indicating most of the Ru^{x+} is reduced to Ru^0 [81,82]. In the XPS spectrum of O 1 s (Fig. 4**j**), the lattice oxygen content reduces significantly compared to the pre-stability test sample [83,84], demonstrating that Cu_2O is reduced to Cu. The cuprous oxide in the catalyst is converted to zero-valent copper after the stability test. While, the stable morphological structure and the successful doping of Ru, ensure that the catalyst has both excellent performance and stability.

The HER performance of the Ru-Cu_2O/CF was carried out in neutral solution (1.0 M PBS). Fig. 5**a, b** exhibited the ultra-low overpotential of Ru-Cu_2O/CF, which driving 10 mA cm^{-2} only needs 51 mV, much lower than Ru/CF (73 mV), Cu/CF (275 mV) and Cu_2O/CF (301 mV). In addition, the overpotential of the Ru-Cu_2O/CF at 100 mA cm^{-2} is only 159 mV, compared to other comparison samples, this sample is much smaller. The Tafel slope (Fig. 5**c**) of Ru-Cu_2O/CF is 58 mV dec^{-1}, which is lesser than Ru/CF (60 mV dec^{-1}), Cu/CF (149 mV dec^{-1}), Cu_2O/CF (143 mV dec^{-1}), $Cu(OH)_2$/CF (229 mV dec^{-1}), and CF (301 mV dec^{-1}) verifying its favorable kinetics for HER. In terms of catalyst stability in 1.0 M PBS is characterized by a chronopotentiometry test over 50,000 s at 10 mA cm^{-2} (Fig. 5**d**). Moreover, after 5000 and 10,000 CV cycles, the LSV curves of the electrocatalytic display a negligible decrease

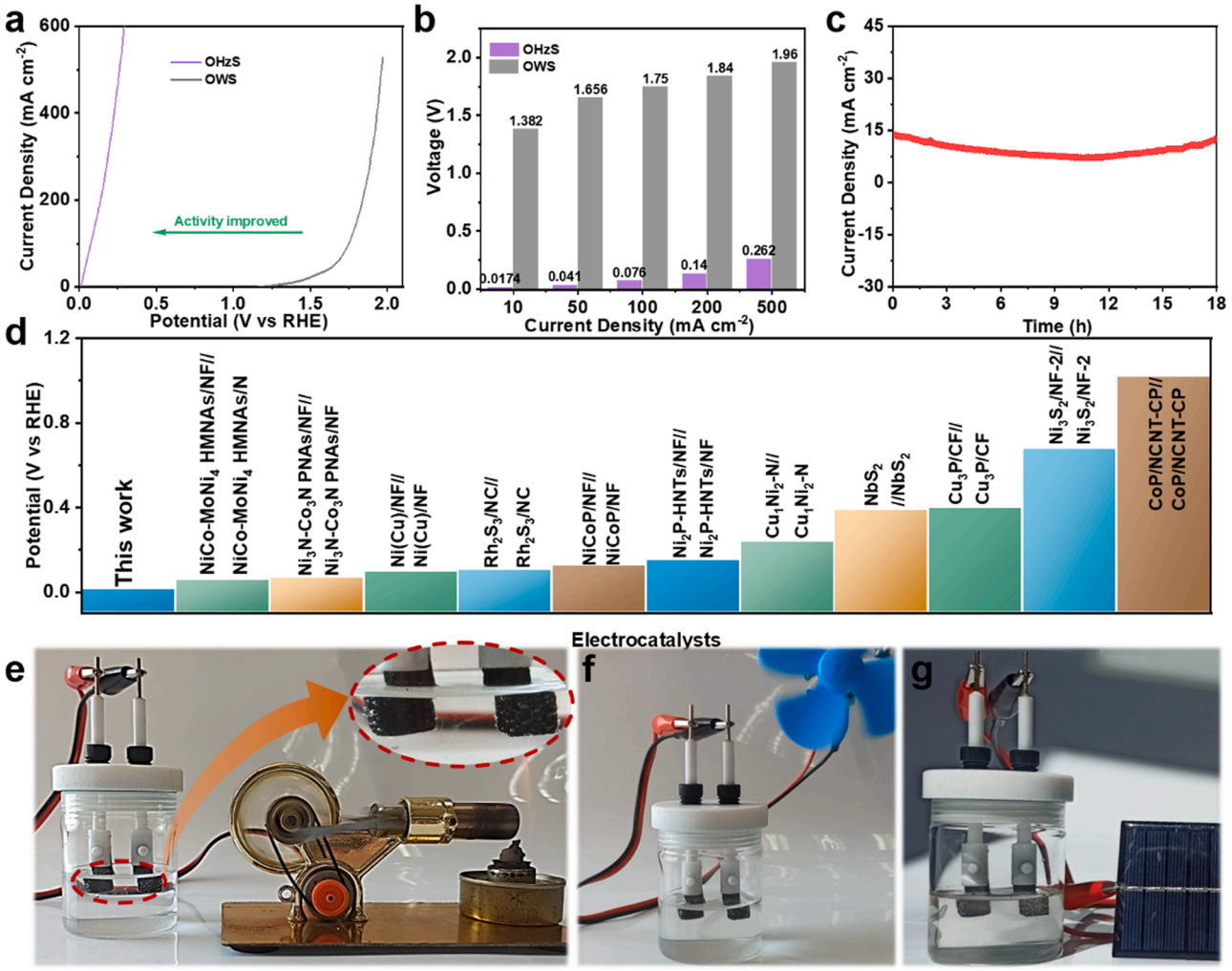

Fig. 7. OHzS performance of the Ru-Cu_2O/CF||Ru-Cu_2O/CF in alkaline solution. (a) The LSV curves of OHzS and OWS. (b) Overpotential of OHzS and OWS at 10–500 mA cm^{-2}. (c) The chronoamperometry curves for Ru-Cu_2O/CF at the voltage of 0.03 V. (d) Comparison overpotentials at 10 mA cm^{-2} of the recently reported catalysts. (e-g) Thermal, wind and solar energy drive the OHzS to product H_2.

(Fig. 5**e**). In addition, the morphology of the Ru-Cu_2O/CF maintains well after 50,000 s chronopotentiometry tests, demonstrating the superior robust structure of Ru-Cu_2O/CF (Fig. S8). Fig. S9 is the XPS Remarkably, the Ru-Cu_2O/CF presents excellent catalytic performance compared with other recently reported Catalysts containing Ru (Fig. 5**f** and Table S2).

3.3. Hydrazine oxidation reaction performance

The electrochemical performance for HzOR is performed in N_2H_4/KOH medium. Likewise, the Ru-Cu_2O/CF also presents the highest catalytic performance for HzOR. As depicted in Fig. 6**a** and **b**, small potentials of − 0.041 V are required to reach 10 mA cm^{-2} for Ru-Cu_2O/CF, that is lower than Ru/CF (0.039 V), Cu/CF (0.027 V), Cu_2O/CF (0.266 V) and $Cu(OH)_2$/CF (0.1 V). Likewise, Ru-Cu_2O/CF only required a potential of − 0.013 V to drive a 100 mA cm^{-2}. Tafel slope of Ru-Cu_2O/CF is merely 34 mV dec^{-1}, whereas Ru/CF is 76 mV dec-1, Cu/CF is 71 mV dec^{-1}, Cu2O/CF is 63 mV dec^{-1}, Cu(OH)2/CF is 83 mV dec^{-1}, and CF is 507 mV dec^{-1}. The smallest Tafel slope means that Ru-Cu_2O/CF has the most favorable reaction kinetics (Fig. 6**c**). Moreover, Ru-Cu_2O/CF has an improved stability as demonstrated by the chronoamperometry test and multistep chronopotentiometry curves, in the Fig. 6**d**. As Fig. 6**e** shows that HzOR owns an excellent kinetic advantage over OER. As shown in Fig. 6**f**, Ru-Cu_2O/CF only needs − 0.041, − 0.027, − 0.013 and 0.086 V to reach 10, 50, 100 and 200 mA cm^{-2} for HzOR. Especially, the as-synthesized Ru-Cu_2O/CF performance surpasses many recently reported electrocatalysts (Fig. 6**g** and Table S3). To investigate its stability, we used the XPS to analyzing chemical composition and structure of the Ru-Cu_2O/CF in the Fig. S10.

3.4. The HzOR-assisted OWS performance

Considering the excellent performance and robust stability of the Ru-Cu_2O/CF for HER and HzOR, we investigated the hybrid water electrolysis performance using a two-electrode cell with Ru-Cu_2O/CF as both anode and cathode. Fig. 7**a, b** shows that OHzS exhibits significant kinetic advantages over OWS. For OHzS, 0.0174, 0.041, 0.076, 0.14 and 0.26 V are required to reach current densities of 10, 50, 100, 200 and 500 mA cm^{-2}, while for OWS are 1.382, 1.656, 1.75, 1.84 and 1.96 V, respectively. Simultaneously, the chronoamperometry curves show the excellent stability of the catalyst, with the current density almost constant before and after the 18 h stability test (Fig. 7**c**). Compared with other recently reported advanced catalysts, the synthesized sample owns min overpotential at 10 mA cm^{-2} (Fig. 7**d** and Table S4). In Fig. 7**e** and Movie S1, the Stirling generator drives an electrolytic cell assembled with Ru-Cu_2O/CF Serving as both cathode and anode in 1.0 M KOH and 0.5 M N_2H_4, respectively. The insert picture shows that the electrode surface is covered with abundant bubbles. The experiment accomplishes

the conversion of thermal energy into hydrogen energy. In addition, hydrogen production from OHzS can be powered by solar panels and fan generators with sumless bubbles generated on both the electrodes (Fig. 7**f, g** and Movie S2, S3).

Supplementary material related to this article can be found online at doi:10.1016/j.jhazmat.2021.126226.

4. Conclusions

In summary, we fabricated a 3D self-supported Ru doped Cu_2O nanochains as difunctional electrocatalysts for HER and HzOR. The unique morphological feature and hydrophilic surface benefit the mass transfer, enhance the electrolyte-electrode contact and boost the reaction kinetics. During the electrocatalytic process Cu-Ru interactions significantly enhance electrocatalytic activity. Impressively, Ru-Cu_2O/CF exhibits superior HER performance in alkaline and neutral electrolytes. In addition, Ru-Cu_2O/CF also has favorable HzOR activity and can be used as a bifunctional electrocatalyst. The simulation experiments have converted wind, solar, and thermal energies to hydrogen energy. This work provides insights for designing excellent metal-doped copper-based OHzS electrocatalyst used for the conversion and storage of energy.

CRediT authorship contribution statement

Pei Shen: Methodology, Investigation, Validation, Writing – original draft, Formal analysis. **Bowen Zhou:** Methodology, Software, Data curation. **Zhi Chen:** Methodology, Software, Data curation. **Weiping Xiao:** valuable guidance and writing assistance. **Yunlei Fu:** valuable guidance and writing assistance. **Jun Wan:** valuable guidance and writing assistance. **Zexing Wu:** Conceptualization, Writing – review & editing, Supervision. **Lei Wang:** Conceptualization, Funding acquisition, Supervision.

Declaration of Competing Interest

The authors declare that they have no known competing financial interests or personal relationships that could have appeared to influence the work reported in this paper.

Data Availability

The authors do not have permission to share data.

Acknowledgments

The authors thank funding support from the National Natural Science Foundation of China (22002068; 52272222, and 52072197), Taishan Scholar Young Talent Program (tsqn201909114), Youth Innovation and Technology Foundation of Shandong Higher Education Institutions, China (2019KJC004), Outstanding Youth Foundation of Shandong Province, China (ZR2019JQ14), Major Basic Research Program of Natural Science Foundation of Shandong Province under Grant No. ZR2020ZD09, Major Scientific and Technological Innovation Project (2019JZZY020405), Project funded by China Postdoctoral Science Foundation (2021M691700), and the Natural Science Foundation of Shandong Province of China (ZR2019BB002; ZR2018BB031), the Postdoctoral Innovation Project of Shandong Province.

Appendix A. Supporting information

Supplementary data associated with this article can be found in the online version at doi:10.1016/j.apcatb.2022.122305.

References

[1] Y. Jia, F. Li, K. Fan, L. Sun, Cu-based bimetallic electrocatalysts for CO_2 reduction, Adv. Powder Mater. 1 (2022), 100012.
[2] Q. Qian, J. Zhang, J. Li, Y. Li, X. Jin, Y. Zhu, Y. Liu, Z. Li, A. El-Harairy, C. Xiao, G. Zhang, Y. Xie, Artificial heterointerfaces achieve delicate reaction kinetics towards hydrogen evolution and hydrazine oxidation catalysis, Angew. Chem. Int. Ed. 60 (2021) 5984–5993.
[3] C. Yang, W. Zhong, K. Shen, Q. Zhang, R. Zhao, H. Xiang, J. Wu, X. Li, N. Yang, Electrochemically reconstructed Cu-FeOOH/Fe_3O_4 catalyst for efficient hydrogen evolution in alkaline media, Adv. Energy Mater. 12 (2022), 2200077.
[4] J. Wang, S. Xin, Y. Xiao, Z. Zhang, Z. Li, W. Zhang, C. Li, R. Bao, J. Peng, J. Yi, S. Chou, Manipulating the water dissociation electrocatalytic sites of bimetallic nickel-based alloys for highly efficient alkaline hydrogen evolution, Angew. Chem. Int. Ed. 61 (2022), e202202518.
[5] J. Lee, H. Jung, Y.S. Park, N. Kwon, S. Woo, N.C.S. Selvam, G.S. Han, H.S. Jung, P. J. Yoo, S.M. Choi, J.W. Han, B. Lim, Chemical transformation approach for high-performance ternary NiFeCo metal compound-based water splitting electrodes, Appl. Catal., B 294 (2021), 120246.
[6] W. Yu, Z. Chen, W. Xiao, Y. Chai, B. Dong, Z. Wu, L. Wang, Phosphorus doped two-dimensional $CoFe_2O_4$ nanobelts decorated with Ru nanoclusters and Co–Fe hydroxide as efficient electrocatalysts toward hydrogen generation, Inorg. Chem. Front. 9 (2022) 1847–1855.
[7] Z. Wu, Y. Zhao, W. Xiao, Y. Fu, B. Jia, T. Ma, L. Wang, Metallic-bonded Pt-Co for atomically dispersed Pt in the Co_4N matrix as an efficient electrocatalyst for hydrogen generation, ACS Nano 16 (2022) 18038–18047.
[8] T. Wu, J. Hong, Z. Lu, H. Wu, C. Wu, Z. Tang, X. Liu, B. Zeng, Y. Xu, G. Chen, C. Yuan, L. Dai, In-situ generation of Ru-catechol coordinative polymer precursor for high-performance hydrogen evolution reaction doped carbon catalyst, Appl. Catal., B 285 (2021), 119795.
[9] Q. Liu, R. Liu, C. He, C. Xia, W. Guo, Z.-L. Xu, B.Y. Xia, Advanced polymer-based electrolytes in zinc-air batteries, eScience 2 (2022) 453–466.
[10] R. Anand, A.S. Nissimagoudar, M. Umer, M. Ha, M. Zafari, S. Umer, G. Lee, K. S. Kim, Late transition metal doped MXenes showing superb bifunctional electrocatalytic activities for water splitting via distinctive mechanistic pathways, Adv. Energy Mater. 11 (2021), 2102388.
[11] J. Wang, Z. Zhang, H. Song, B. Zhang, J. Liu, X. Shai, L. Miao, Water dissociation kinetic-oriented design of nickel sulfides via tailored dual sites for efficient alkaline hydrogen evolution, Adv. Funct. Mater. 31 (2021), 2008578.
[12] Y. Niu, S. Gong, X. Liu, C. Xu, M. Xu, S.-G. Sun, Z. Chen, Engineering iron-group bimetallic nanotubes as efficient bifunctional oxygen electrocatalysts for flexible Zn-air batteries, eScience 2 (2022) 546–556.
[13] D. Wang, Q. Li, C. Han, Q. Lu, Z. Xing, X. Yang, Atomic and electronic modulation of self-supported nickel-vanadium layered double hydroxide to accelerate water splitting kinetics, Nat. Commun. 10 (2019) 3899.
[14] B. You, X. Liu, N. Jiang, Y. Sun, A general strategy for decoupled hydrogen production from water splitting by integrating oxidative biomass valorization, J. Am. Chem. Soc. 138 (2016) 13639–13646.
[15] Z. Wang, L. Xu, F. Huang, L. Qu, J. Li, K.A. Owusu, Z. Liu, Z. Lin, B. Xiang, X. Liu, K. Zhao, X. Liao, W. Yang, Y.-B. Cheng, L. Mai, Copper-nickel nitride nanosheets as efficient bifunctional catalysts for hydrazine-assisted electrolytic hydrogen production, Adv. Energy Mater. 9 (2019), 1900390.
[16] J. Zhang, Z. Zhao, Z. Xia, L. Dai, A metal-free bifunctional electrocatalyst for oxygen reduction and oxygen evolution reactions, Nat. Nanotechnol. 10 (2015) 444–452.
[17] Z.-F. Huang, J. Song, Y. Du, S. Xi, S. Dou, J.M.V. Nsanzimana, C. Wang, Z.J. Xu, X. Wang, Chemical and structural origin of lattice oxygen oxidation in Co-Zn oxyhydroxide oxygen evolution electrocatalysts, Nat. Energy 4 (2019) 329–338.
[18] Y. Liu, J. Zhang, Y. Li, Q. Qian, Z. Li, G. Zhang, Realizing the synergy of interface engineering and chemical substitution for Ni3N enables its bifunctionality toward hydrazine oxidation assisted energy-saving hydrogen production, Adv. Funct. Mater. 31 (2021), 2103673.
[19] H. Niu, C. Xia, L. Huang, S. Zaman, T. Maiyalagan, W. Guo, B. You, B.Y. Xia, Rational design and synthesis of one-dimensional platinum-based nanostructures for oxygen-reduction electrocatalysis, Chin. J. Catal. 43 (2022) 1459–1472.
[20] Q. Qian, J. Zhang, J. Li, Y. Li, X. Jin, Y. Zhu, Y. Liu, Z. Li, A. El-Harairy, C. Xiao, G. Zhang, Y. Xie, Artificial heterointerfaces achieve delicate reaction kinetics towards hydrogen evolution and hydrazine oxidation catalysis, Angew. Chem. Int. Ed. 60 (2021) 5984–5993.
[21] X. Guo, X. Wan, Q. Liu, Y. Li, W. Li, J. Shui, Phosphated IrMo bimetallic cluster for efficient hydrogen evolution reaction, eScience 2 (2022) 304–310.
[22] X.-P.L. En-Hui Ma, Tao Shen, De-Li Wang, Constructing carbon-encapsulated NiFeV-based electrocatalysts by alkoxide-based self-template method for oxygen evolution reaction, Acta Phys. -Chim. Sin. 37 (2021), 2010029.
[23] Z. Li, X. Jiang, X. Wang, J. Hu, Y. Liu, G. Fu, Y. Tang, Concave PtCo nanocrosses for methanol oxidation reaction, Appl. Catal., B 277 (2020), 119135.
[24] S. Chen, D. Huang, D. Liu, H. Sun, W. Yan, J. Wang, M. Dong, X. Tong, W. Fan, Hollow and porous $NiCo_2O_4$ nanospheres for enhanced methanol oxidation reaction and oxygen reduction reaction by oxygen vacancies engineering, Appl. Catal., B 291 (2021), 120065.
[25] B. Zhu, Z. Liang, R. Zou, Designing advanced catalysts for energy conversion based on urea oxidation reaction, Small 16 (2020), 1906133.
[26] S. Ni, H. Qu, Z. Xu, X. Zhu, H. Xing, L. Wang, J. Yu, H. Liu, C. Chen, L. Yang, Interfacial engineering of the $NiSe_2$/$FeSe_2$ p-p heterojunction for promoting oxygen evolution reaction and electrocatalytic urea oxidation, Appl. Catal. B 299 (2021), 120638.

[27] Y. Zhu, X. Zhu, L. Bu, Q. Shao, Y. Li, Z. Hu, C.-T. Chen, C.-W. Pao, S. Yang, X. Huang, Single-atom in-doped subnanometer pt nanowires for simultaneous hydrogen generation and biomass upgrading, Adv. Funct. Mater. 30 (2020), 2004310.

[28] E. Tayyebi, Á.B. Höskuldsson, A. Wark, N. Atrak, B.M. Comer, A.J. Medford, E. Skúlason, Perspectives on the competition between the electrochemical water and N_2 oxidation on a TiO_2(110) electrode, J. Phys. Chem. C. 13 (2022) 6123–6129.

[29] N.K. Katiyar, S. Dhakar, A. Parui, P. Gakhad, A.K. Singh, K. Biswas, C.S. Tiwary, S. Sharma, Electrooxidation of hydrazine utilizing high-entropy alloys: assisting the oxygen evolution reaction at the thermodynamic voltage, ACS Catal. 11 (2021) 14000–14007.

[30] Y. Yu, S.J. Lee, J. Theerthagiri, Y. Lee, M.Y. Choi, Architecting the AuPt alloys for hydrazine oxidation as an anolyte in fuel cell: comparative analysis of hydrazine splitting and water splitting for energy-saving H_2 generation, Appl. Catal. B 316 (2022), 121603.

[31] J. Li, C. Dong, M. Guo, W. Gao, L. Kang, F. Lei, P. Hao, J. Xie, B. Tang, Cerium-induced lattice disordering in Co-based nanocatalysts promoting the hydrazine electro-oxidation behavior, Chem. Commun. 58 (2022) 6845–6848.

[32] J. Hou, X. Peng, J. Sun, S. Zhang, Q. Liu, X. Wang, J. Luo, X. Liu, Accelerating hydrazine-assisted hydrogen production kinetics with Mn dopant modulated CoS_2 nanowire arrays, Inorg. Chem. Front. 9 (2022) 3047–3058.

[33] X. Xu, T. Wang, L. Dong, W. Lu, X. Miao, Energy-efficient hydrogen evolution reactions via hydrazine oxidation over facile synthesis of cobalt tetraoxide electrodes, ACS Sustain. Chem. Eng. 8 (2020) 7973–7980.

[34] J. Li, S. Wang, J. Chang, L. Feng, A review of Ni based powder catalyst for urea oxidation in assisting water splitting reaction, Adv. Powder Mater. 1 (2022), 100030.

[35] J. Xie, X. Yang, Y. Wang, L. Kang, J. Li, Z. Wei, P. Hao, F. Lei, Q. Wang, B. Tang, "Pit-dot" ultrathin nanosheets of hydrated copper pyrophosphate as efficient pre-catalysts for robust water oxidation, Chem. Commun. 57 (2021) 11517–11520.

[36] X. Yang, L. Kang, Z. Wei, S. Lou, F. Lei, P. Hao, J. Xie, B. Tang, A self-sacrificial templated route to fabricate CuFe Prussian blue analogue/$Cu(OH)_2$ nanoarray as an efficient pre-catalyst for ultrastable bifunctional electro-oxidation, Chem. Eng. J. 422 (2021), 130139.

[37] X.-W. Lv, Q. Kong, X.-L. Song, Y. Liu, Z.-Y. Yuan, Coupling nonstoichiometric $Cu_{2-x}Se$ with stable Cu_2Se berzelianite for efficient synergistic electrocatalytic hydrazine-assisted water splitting, Inorg. Chem. Front. 9 (2022) 6182–6189.

[38] L. Xiao, G. Li, Z. Yang, K. Chen, R. Zhou, H. Liao, Q. Xu, J. Xu, Engineering of amorphous PtOx interface on Pt/WO_3 nanosheets for ethanol oxidation electrocatalysis, Adv. Funct. Mater. 31 (2021), 2100982.

[39] L. Gao, J. Xie, S. Liu, S. Lou, Z. Wei, X. Zhu, B. Tang, Crystalline Cobalt/Amorphous $LaCoO_x$ hybrid nanoparticles embedded in porous nitrogen-doped carbon as efficient electrocatalysts for hydrazine-assisted hydrogen production, ACS Appl. Mater. Interfaces 12 (2020) 24701–24709.

[40] J. Xie, J. Qi, F. Lei, Y. Xie, Modulation of electronic structures in two-dimensional electrocatalysts for the hydrogen evolution reaction, Chem. Commun. 56 (2020) 11910–11930.

[41] Y.-N. Zhou, Y.-R. Zhu, X.-T. Yan, Y.-N. Cao, J. Li, B. Dong, M. Yang, Q.-Z. Li, C.-G. Liu, Y.-M. Chai, Hierarchical CoSeS nanostructures assisted by Nb doping for enhanced hydrogen evolution reaction, Chin. J. Catal. 42 (2021) 431–438.

[42] W. Yu, Y. Gao, Z. Chen, Y. Zhao, Z. Wu, L. Wang, Strategies on improving the electrocatalytic hydrogen evolution performances of metal phosphides, Chin. J. Catal. 42 (2021) 1876–1902.

[43] Y. Gao, D. Zheng, Q. Li, W. Xiao, T. Ma, Y. Fu, Z. Wu, L. Wang, 3D Co_3O_4-RuO_2 hollow spheres with abundant interfaces as advanced trifunctional electrocatalyst for water-splitting and flexible Zn–Air battery, Adv. Funct. Mater. 32 (2022), 2203206.

[44] Y. Liu, X. Luo, C. Zhou, S. Du, D. Zhen, B. Chen, J. Li, Q. Wu, Y. Iru, D. Chen, A modulated electronic state strategy designed to integrate active HER and OER components as hybrid heterostructures for efficient overall water splitting, Appl. Catal., B 260 (2020), 118197.

[45] T. Zhang, B. Zhang, Q. Peng, J. Zhou, Z. Sun, Mo_2B_2 MBene-supported single-atom catalysts as bifunctional HER/OER and OER/ORR electrocatalysts, J. Mater. Chem. A 9 (2021) 433–441.

[46] W. Liu, J. Xie, Y. Guo, S. Lou, L. Gao, B. Tang, Sulfurization-induced edge amorphization in copper-nickel-cobalt layered double hydroxide nanosheets promoting hydrazine electro-oxidation, J. Mater. Chem. A 7 (2019) 24437–24444.

[47] C. Panda, P.W. Menezes, M. Zheng, S. Orthmann, M. Driess, In situ formation of nanostructured core-shell Cu_3N-CuO to promote alkaline water electrolysis, ACS Energy Lett. 4 (2019) 747–754.

[48] L. Yan, B. Zhang, J. Zhu, Y. Li, P. Tsiakaras, P. Kang Shen, Electronic modulation of cobalt phosphide nanosheet arrays via copper doping for highly efficient neutral-pH overall water splitting, Appl. Catal., B 265 (2020), 118555.

[49] X. Wang, S. Liu, H. Zhang, S. Zhang, G. Meng, Q. Liu, Z. Sun, J. Luo, X. Liu, Polycrystalline SnSx nanofilm enables CO_2 electroreduction to formate with high current density, Chem. Commun. 58 (2022) 7654–7657.

[50] L. Li, I.Mu Hasan, Farwa, R. He, L. Peng, N. Xu, N.K. Niazi, J.-N. Zhang, J. Qiao, Copper as a single metal atom based photo-, electro-, and photoelectrochemical catalyst decorated on carbon nitride surface for efficient CO_2 reduction: a review, Nano Res. Energy 1 (2022), e9120015.

[51] L. Yu, H. Zhou, J. Sun, F. Qin, F. Yu, J. Bao, Y. Yu, S. Chen, Z. Ren, Cu nanowires shelled with NiFe layered double hydroxide nanosheets as bifunctional electrocatalysts for overall water splitting, Energy Environ. Sci. 10 (2017) 1820–1827.

[52] W.-J. Kang, Y. Feng, Z. Li, W.-Q. Yang, C.-Q. Cheng, Z.-Z. Shi, P.-F. Yin, G.-R. Shen, J. Yang, C.-K. Dong, H. Liu, F.-X. Ye, X.-W. Du, Strain-activated copper catalyst for pH-universal hydrogen evolution reaction, Adv. Funct. Mater. 32 (2022), 2112367.

[53] P. Shen, T. Yang, Q. Li, Z. Chen, Y. Wang, Y. Fu, J. Wan, Z. Wu, L. Wang, Hollow-structured amorphous $Cu(OH)_x$ nanowires doped with Ru for wide pH electrocatalytic hydrogen production, J. Colloid Interface Sci. 628 (2022) 1061–1069.

[54] C. Song, Z. Zhao, X. Sun, Y. Zhou, Y. Wang, D. Wang, In situ growth of Ag nanodots decorated Cu_2O porous nanobelts networks on copper foam for efficient HER electrocatalysis, Small 15 (2019), 1804268.

[55] U.Y. Qazi, R. Javaid, N. Tahir, A. Jamil, A. Afzal, Design of advanced self-supported electrode by surface modification of copper foam with transition metals for efficient hydrogen evolution reaction, Int. J. Hydrog. Energy 45 (2020) 33396–33406.

[56] S.Z. Tianran Wei, Qian Liu, Yuan Qiu, Jun Luo, Xijun Liu, Oxygen vacancy-rich amorphous copper oxide enables highly selective electroreduction of carbon dioxide to ethylene, Acta Phys. Chim. Sin. 39 (2023), 2207026.

[57] T. Ahmad, S. Liu, M. Sajid, K. Li, M. Ali, L. Liu, W. Chen, Electrochemical CO_2 reduction to C^{2+} products using Cu-based electrocatalysts: a review, Nano Res. Energy 1 (2022), e9120021.

[58] D.T. Tran, H.T. Le, T.L. Luyen Doan, N.H. Kim, J.H. Lee, Pt nanodots monolayer modified mesoporous Cu@Cu_xO nanowires for improved overall water splitting reactivity, Nano Energy 59 (2019) 216–228.

[59] H. Xu, T. Liu, S. Bai, L. Li, Y. Zhu, J. Wang, S. Yang, Y. Li, Q. Shao, X. Huang, Cation exchange strategy to single-atom noble-metal doped CuO nanowire arrays with ultralow overpotential for H_2O splitting, Nano Lett. 20 (2020) 5482–5489.

[60] T. Wu, J. Hong, Z. Lu, H. Wu, C. Wu, Z. Tang, X. Liu, B. Zeng, Y. Xu, G. Chen, C. Yuan, L. Dai, In-situ generation of Ru-catechol coordinative polymer precursor for high-performance hydrogen evolution reaction doped carbon catalyst, Appl. Catal., B 285 (2021) 119795.

[61] P. Su, W. Pei, X. Wang, Y. Ma, Q. Jiang, J. Liang, S. Zhou, J. Zhao, J. Liu, G.Q. Lu, Exceptional electrochemical HER performance with enhanced electron transfer between Ru nanoparticles and single atoms dispersed on a carbon substrate, Angew. Chem. Int. Ed. 60 (2021) 16044–16050.

[62] H. Huang, H. Jung, S. Li, S. Kim, J.W. Han, J. Lee, Activation of inert copper for significantly enhanced hydrogen evolution behaviors by trace ruthenium doping, Nano Energy 92 (2022), 106763.

[63] F. He, N. Xia, Y. Zheng, Y. Zhang, H. Fan, D. Ma, Q. Liu, X. Hu, In situ electrochemical fabrication of ultrasmall Ru-based nanoparticles for robust N_2H_4 oxidation, ACS Appl. Mater. Interfaces 13 (2021) 8488–8496.

[64] J. Li, C. Zhang, C. Zhang, H. Ma, Y. Yang, Z. Guo, Y. Wang, H. Ma, Electronic configuration of single ruthenium atom immobilized in urchin-like tungsten trioxide towards hydrazine oxidation-assisted hydrogen evolution under wide pH media, Chem. Eng. J. 430 (2022), 132953.

[65] J. Wang, X. Guan, H. Li, S. Zeng, R. Li, Q. Yao, H. Chen, Y. Zheng, K. Qu, Robust Ru-N metal-support interaction to promote self-powered H2 production assisted by hydrazine oxidation, Nano Energy 100 (2022), 107467.

[66] Y. Xu, K. Ren, T. Ren, M. Wang, Z. Wang, X. Li, L. Wang, H. Wang, Ultralow-content Pd in-situ incorporation mediated hierarchical defects in corner-etched Cu_2O octahedra for enhanced electrocatalytic nitrate reduction to ammonia, Appl. Catal., B 306 (2022), 121094.

[67] J. Li, C. Guo, L. Li, Y. Gu, K. BoK-Hee, J. Huang, Construction of Z-scheme WO_3-Cu_2O nanorods array heterojunction for efficient photocatalytic degradation of methylene blue, Inorg. Chem. Commun. 138 (2022), 109248.

[68] L. Zhang, Y. Meng, H. Shen, J. Li, C. Yang, B. Xie, S. Xia, High-efficiency photocatalytic ammonia synthesis by facet orientation-supported heterojunction Cu_2O@BiOCl [100] boosted by double built-in electric fields, Inorg. Chem. 61 (2022) 6045–6055.

[69] G. Sun, S. Jia, X. Zhang, Z. Kang, M. Cui, B. Wang, B. Wang, D.-P. Yang, Anchoring core-shell Cu@Cu_2O nanoparticles to two-dimensional carbon nanosheets for bacterial disinfection, ACS Appl. Nano Mater. 4 (2021) 9831–9841.

[70] Y. Deng, L. Tang, G. Zeng, C. Feng, H. Dong, J. Wang, H. Feng, Y. Liu, Y. Zhou, Y. Pang, Plasmonic resonance excited dual Z-scheme $BiVO_4$/Ag/Cu_2O nanocomposite: synthesis and mechanism for enhanced photocatalytic performance in recalcitrant antibiotic degradation, Environ. Sci.: Nano 4 (2017) 1494–1511.

[71] H. Luo, B. Li, J.-G. Ma, P. Cheng, Surface modification of Nano-Cu_2O for Controlling CO_2 electrochemical reduction to ethylene and syngas, Angew. Chem. Int. Ed. 61 (2022), e202116736.

[72] S. Hao, G. Zheng, S. Gao, L. Qiu, N. Xu, Y. He, L. Lei, X. Zhang, In situ synthesis of ternary NiCoRu-based layered double hydroxide by chlorine corrosion toward electrocatalytic water oxidation, ACS Sustain. Chem. Eng. 7 (2019) 14361–14367.

[73] G. Meng, H. Tian, L. Peng, Z. Ma, Y. Chen, C. Chen, Z. Chang, X. Cui, J. Shi, Ru to W electron donation for boosted HER from acidic to alkaline on Ru/WNO sponges, Nano Energy 80 (2021), 105531.

[74] J. Zhang, X. Mao, S. Wang, L. Liang, M. Cao, L. Wang, G. Li, Y. Xu, X. Huang, Superlattice in a Ru superstructure for enhancing hydrogen, Evol., Angew. Chem. Int. Ed. 61 (2022), e202116867.

[75] X. Mu, X. Gu, R. Zhou, L. Li, G. Lu, C. Chen, S. Liu, S. Mu, W. Chen, Metastable five-fold twinned Ru incorporated Cu nanosheets with Pt-like hydrogen evolution kinetics, Chem. Eng. J. 428 (2022), 131099.

[76] W. Niu, T. Moehl, P. Adams, X. Zhang, R. Lefèvre, A.M. Cruz, P. Zeng, K. Kunze, W. Yang, S.D. Tilley, Crystal orientation-dependent etching and trapping in thermally-oxidised Cu_2O photocathodes for water splitting, Energy Environ. Sci. 15 (2022) 2002–2010.

[77] J. He, D.W. Shao, L.C. Zheng, L.J. Zheng, D.Q. Feng, J.P. Xu, X.H. Zhang, W. C. Wang, W.H. Wang, F. Lu, H. Dong, Y.H. Cheng, H. Liu, R.K. Zheng, Construction of Z-scheme Cu_2O/Cu/AgBr/Ag photocatalyst with enhanced photocatalytic activity and stability under visible light, Appl. Catal., B 203 (2017) 917–926.
[78] S. Ge, L. Zhang, J. Hou, S. Liu, Y. Qin, Q. Liu, X. Cai, Z. Sun, M. Yang, J. Luo, X. Liu, Cu_2O-derived PtCu nanoalloy toward energy-efficient hydrogen production via hydrazine electrolysis under large current density, ACS Appl. Energy Mater. 5 (2022) 9487–9494.
[79] H. Zhang, Y. Luo, P.K. Chu, Q. Liu, X. Liu, S. Zhang, J. Luo, X. Wang, G. Hu, Recent advances in non-noble metal-based bifunctional electrocatalysts for overall seawater splitting, J. Alloy. Compd. 922 (2022), 166113.
[80] J. Ding, H. Yang, S. Zhang, Q. Liu, H. Cao, J. Luo, X. Liu, Advances in the electrocatalytic hydrogen evolution reaction by metal nanoclusters-based materials, Small (2022), 2204524.
[81] G. Liu, W. Zhou, B. Chen, Q. Zhang, X. Cui, B. Li, Z. Lai, Y. Chen, Z. Zhang, L. Gu, H. Zhang, Synthesis of RuNi alloy nanostructures composed of multilayered nanosheets for highly efficient electrocatalytic hydrogen evolution, Nano Energy 66 (2019), 104173.
[82] M. Li, H. Wang, W. Zhu, W. Li, C. Wang, X. Lu, RuNi nanoparticles embedded in N-doped carbon nanofibers as a robust bifunctional catalyst for efficient overall water splitting, Adv. Sci. 7 (2020), 1901833.
[83] H. Guan, P. Cai, X. Zhang, Y. Zhang, G. Chen, C. Dong, Cu2O templating strategy for the synthesis of octahedral Cu_2O@$Mn(OH)_2$ core–shell hierarchical structures with a superior performance supercapacitor, J. Mater. Chem. A 6 (2018) 13668–13675.
[84] Z. Ma, K. Rui, Q. Zhang, Y. Zhang, M. Du, D. Li, Q. Wang, X. Huang, J. Zhu, W. Huang, Self-templated formation of uniform F-CuO hollow octahedra for lithium ion batteries, Small 13 (2017), 1603500.